Hindawi
Journal of Chemistry
Volume 2019, Article ID 4932837, 10 pages
https://doi.org/10.1155/2019/4932837

Research Article

Adsorption Characteristics and Transport Behavior of Cr(VI) in Shallow Aquifers Surrounding a Chromium Ore Processing Residue (COPR) Dumpsite

Yu Liu,[1,2] **Yin Li**,[2] **Yucheng Hu**,[2] **Khan M. G. Mostofa**,[1] **Siliang Li**,[1] **and Zhenying Liu**[3]

[1]*Institute of Surface-Earth System Science, Tianjin University, Weijin Road 92, Tianjin 300072, China*
[2]*Tianjin Hydraulic Science Research Institute, Youyi Road 60, Tianjin 300061, China*
[3]*School of Environmental Science and Safety Engineering, Tianjin University of Technology, Tianjin 300191, China*

Correspondence should be addressed to Yu Liu; liuyu2017@tju.edu.cn

Received 26 August 2019; Accepted 3 October 2019; Published 3 November 2019

Guest Editor: Yifeng Zhang

This study explored the stratigraphic distribution and soil/shallow aquifer characteristics surrounding a chromium ore processing residue (COPR) dumpsite at a former chemical factory in China. Total Cr levels in top soils (5–10 cm) nearby the COPR dumpsite were in the range of 8571.4–10711.4 mg/kg. Shallow aquifers (1–6 m) nearby the COPR dumpsite showed a maximum total Cr level of 9756.7 mg/kg. The concentrations of Cr(VI) in groundwater nearby the COPR dumpsite were 766.9–1347.5 mg/L. These results display that the top soils, shallow aquifers, and groundwater of the study site are severely polluted by Cr(VI). Then, three aquifers (silt, clay, and silty clay), respectively, collected from the depth of 1.4–2.4 m, 2.4–4.8 m, and 4.8–11.00 m were first used to evaluate the adsorption characteristics and transport behavior of Cr(VI) in shallow aquifers by both batch and column experiments. The adsorption of Cr(VI) on tested aquifers was well described by pseudo-second-order equation and Freundlich model. The adsorption capacities of Cr(VI) on three aquifers followed the order: clay > silty clay > silt. The kinetics proved that Cr(VI) is not easily adsorbed by the aquifer mediums but transports with groundwater. Thermodynamics indicated that Cr(VI) adsorption on tested aquifers was feasible, spontaneous, and endothermic. Cr(VI) adsorption on tested aquifers decreased with increasing pH. Furthermore, the transport of Cr(VI) in adsorption columns followed the sequence of clay < silty clay < silt. Desorption column experiments infer that the Cr(VI) adsorbed on aquifers will desorb and release into groundwater in the case of rainwater leaching. Therefore, a proper treatment of the COPR and a comprehensive management of soils are vital to prevent groundwater pollution.

1. Introduction

Chromium (Cr) is widely used in various chemical industries, such as electroplating, steelmaking, metallurgy, leather tanning, pigment manufacturing, wood preservative, and textile dyeing [1]. Hexavalent chromium (Cr(VI)) and trivalent chromium (Cr(III)) are the most stable species of Cr in the environment [2]. Cr(III) is relatively stable and has low solubility and mobility in soils and aquifers [3]. On the contrary, Cr(VI) is a strong oxidant and highly mobile, thereby causing Cr(VI) more environmentally available than Cr(III) [4]. Cr(VI) exposure could cause skin irritation, respiratory cancer, and kidney damage [5]. The contamination of soils and groundwater with Cr(VI) has posed a chronic public health and environmental threat due to its high solubility, mobility, toxicity, and mutagenic and carcinogenic properties [6]. The drinking water standard for total Cr of US EPA is 100 μg/L [7]. The permitted concentration of Cr(VI) in drinking water based on the World Health Organization (WHO) guideline is 0.05 mg/L [8].

Chromium ore processing residue (COPR), because of its high content of dissolvable Cr(VI), is one of the most hazardous solid wastes [9]. The continuous Cr(VI) leaching from COPR could cause severe pollution to its surrounding environment, including groundwater [6, 10]. It was reported that only 100 million tons of COPR were treated in China

from 2005 to 2010, yet 300 million tons of COPR still harm the environment [11]. Former Tianjin Tongsheng Chemical Factory started to produce chromate in 1958, which was one of the pioneer chemical factories in China. Even though the factory was shut down in 1998, more than 400 kilotons of COPR were piled up in the open air (just covered by black cloth) in the southwest corner of the factory till 2012. According to our site investigation during 2014 and 2015, there was still significant COPR stored in the factory which has not been properly disposed. Given the large quantity of COPR being placed in the open air for several decades, the continuous Cr(VI) leaching by rain endangers the public health of local residents. It is therefore vital to investigate the distribution, adsorption, and transport of Cr(VI) in surrounding soils and aquifers nearby the COPR dumpsite. However, to the best of our knowledge, no study has been reported in that regards.

Heavy metals in soils may undergo several processes: adsorption/desorption, precipitation/dissolution, oxidation/reduction, plant uptake, microbial conversion, and transport through the soil profile [12]. Although these processes can occur simultaneously, adsorption was the most dominating process controlling existence of metals in soils [12]. Many studies reported about metal adsorption in soil, but fewer studies combine adsorption batch experiments with adsorption/desorption column experiments to investigate the adsorption characteristics and transport behavior of heavy metal in soil and its risk to groundwater. Although many studies were about the Cr(VI) adsorption in soils, previous research studies focused on the adsorption of Cr(VI) in top soils (e.g., 0–6 cm depth [13] and 0–20 cm depth [14–17]), only limited studies reported the adsorption of Cr(VI) in aquifers [18, 19]. However, the adsorption and desorption of Cr(VI) by aquifer mediums are different from the top soils, which are affected by their different geochemical characteristics. In addition, compared with batch experiments of adsorption, only limited studies applied column experiments [14, 16, 17] and 3D sandbox [11] to investigate the transport behavior of Cr(VI) in soils. Desorption experiments were also not carried out in aforementioned column experiments [14, 16, 17]. And rarely works have used real shallow aquifers to fill up columns or sandboxes to investigate the transport behavior of Cr(VI) in aquifers.

In this work, we measured the concentrations of Cr(VI) in top soils (5–10 cm), shallow aquifers and groundwater nearby the COPR dumpsite and explored the stratigraphic distribution and soil characteristics of the study site. Then, three kinds of aquifers were first used to evaluate the adsorption characteristics and transport behavior of Cr(VI) in shallow aquifers by both batch and column experiments. The objectives of the present work were to (1) evaluate the concentrations of Cr(VI) in top soils, shallow aquifers, and groundwater nearby the COPR dumpsite, (2) investigate the adsorption characteristics of Cr(VI) in different aquifers and gain insight into the adsorption mechanism of Cr(VI) in these aquifers, and (3) reveal the adsorption-desorption behaviors of Cr(VI) in aquifers by dynamic column studies. The results of our study can be used to predict the fate and transport behavior of Cr(VI) in polluted soils and aquifers, which will also be helpful to value the risk of contaminant migration and to establish effective remediation plans for contaminated soils.

2. Materials and Methods

2.1. Study Site and Sampling. Geological and hydrogeochemical investigations were carried out near the COPR dumpsite (see Supplementary Material Figure S1) of the former Tianjin Tongsheng Chemical Factory, Tianjin, China. The COPR dumpsite lies at latitude 39°14′21.4″N and longitude 117°06′28.3″E. The topography is alluvial and coastal plain. Eleven sampling sites at different distances from the COPR dumpsite were set to carry out drilling sampling. Schematic of sampling sites is shown in Figure 1. Geographical locations of the drilling sampling sites (Table S1), photographs of core drilling and groundwater sampling (Figure S2), and other detailed information of sampling are all described in the Supplementary Material.

2.2. Stratigraphic Distribution and Soil Characteristics. Based on the Standard for Engineering Classification of Soil (GB/T 50145-2007) [20] and Technical Specification for Division of Subsoil Sequence in Tianjin (DB/T29-191-2009) [21], soils and aquifers within 20 m depth of the study site are divided into 5 layers according to the formation time. From top to bottom, the 5 layers are composed of the artificial fill layer (Qml): the new alluvium (Q_4^{3N}al), the Holocene upper-group lagoon-facies sedimentary layer (Q_4^3 l + h), the Holocene middle-group marine-facies sedimentary layer (Q_4^2m), and the Holocene lower-group continental-facies alluvium (Q_4^1al). The vertical distribution of local geological formations is shown in Table S2. The detailed information of soil and aquifers characteristics is described in the Supplementary Material.

The aquifers used in this study included silt, clay, and silty clay, which were respectively collected from the depth of 1.4–2.4 m, 2.4–4.8 m, and 4.8–11.00 m. At this point, it should be noted that the depth of the groundwater fluctuates between 0.7 m and 1.4 m in our study site. Hence, it is more appropriate to address the silt, clay, and silty clay used in this study as "aquifers" rather than "soils." Therefore, the term "aquifers" will be used in this text to denote silt, clay, and silty clay.

2.3. Experiments. The experiments include batch study and column study. A schematic diagram of the column setup is depicted in Figure S3. The packing status of columns and operating conditions for the adsorption/desorption column experiments are mentioned in Table S3. Also, detailed information of experiments is described in the Supplementary Material.

3. Results and Discussion

3.1. High Concentration of Cr(VI) in Top Soils, Shallow Aquifers, and Groundwater. Drillcore samples were analyzed to determine the stratigraphic distribution and soil

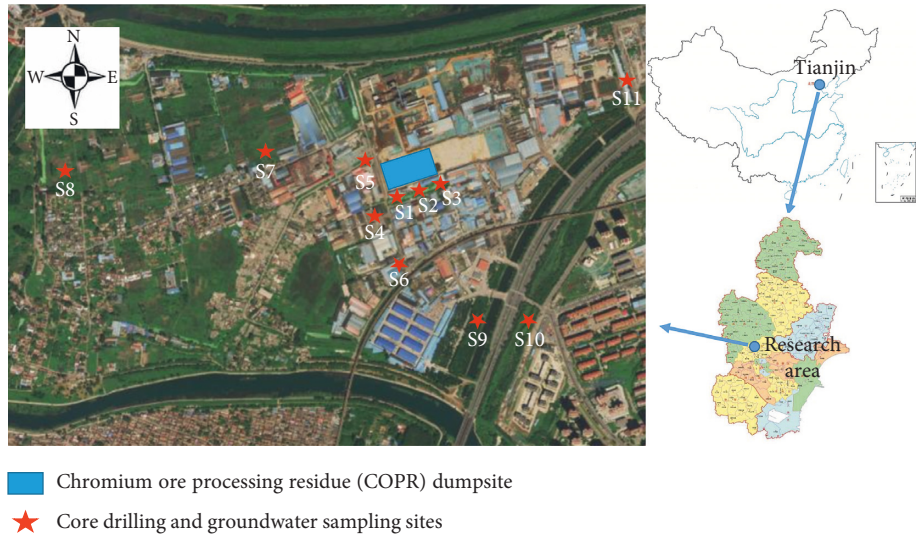

Figure 1: Schematic of sampling sites near the chromium ore processing residue (COPR) dumpsite.

characteristics of the study site. The aquifers (silt, clay, and silty clay) used in this study were collected from the depth of 1.4–2.4 m, 2.4–4.8 m, and 4.8–11.0 m, respectively. Also, the detailed stratigraphic distribution has been discussed in Materials and Methods section. The physicochemical properties of different aquifers are shown in Table S4. The concentrations of total Cr in top soils (5–10 cm) and shallow aquifers (1–6 m) of 11 drilling sampling sites are, respectively, shown in Figures S4 and S5. The concentrations of total Cr in top soils (5–10 cm) nearby the COPR dumpsite (sampling sites S1–S3) were in the range of 8571.4–10711.4 mg/kg. Shallow aquifers (1–6 m) nearby the COPR dumpsite also present high levels of total Cr. Most samples of shallow aquifers (1–6 m) at sampling sites of S1–S6 show high concentrations of total Cr, which were much higher than the Environmental Quality Standard for Soils (250 mg/kg) (GB 15618-2018) [22]. The maximum total Cr level (9756.7 mg/kg) appears at the depth of 1 m at sampling site S2, which was 160 times higher than the background value of Chinese soils (61 mg/kg) [23]. The concentrations of total Cr decrease with increasing depth at most of the sampling sites. Moreover, the concentrations of total Cr at sampling sites of S1–S5 were much higher than those at S6–S11, showing that the shallow aquifers nearer the COPR dumpsite are more severely polluted. The concentrations of Cr(VI) and total Cr of groundwater in 11 monitoring wells are shown in Table S5. The Cr(VI) concentrations of groundwater (monitoring wells S1–S3) nearby the COPR dumpsite range from 766.9 to 1347.5 mg/L, which significantly exceeded the V grade value (0.1 mg/L) of Quality Standard for Groundwater (GB/T 14848-2017) [24] and drinking water standard (0.05 mg/L) of WHO guideline [8]. The pH values of groundwater range from 7.5 to 8.2, which were alkalescent. These results suggest that the top soils (5–10 cm), shallow aquifers (1–6 m), and groundwater nearby the COPR dumpsite are severely contaminated and should get great concern.

3.2. Adsorption Characteristics

3.2.1. Adsorption Kinetics. The adsorption kinetics experiments were studied at pH 7-8, 288 K, and an initial Cr(VI) concentration of 1.0 mg/L. The adsorption kinetics of Cr(VI) in three kinds of aquifers are shown in Figure 2(a). The Cr(VI) adsorption was fast in the first 120 min and then increased slightly until reaching the equilibrium at 240 min. The adsorption capacities of Cr(VI) at the equilibrium time were 1.22, 0.94, and 0.81 mg/kg for clay, silty clay, and silt, respectively. The maximum adsorption rates of Cr(VI) in clay, silty clay, and silt were only 11.9%, 9.3%, and 7.9%, respectively. It demonstrates that Cr(VI) is not easily adsorbed by the aquifer mediums but transports with groundwater, causing long-distance pollution.

To better understand the adsorption kinetics, the pseudo-first-order (PFO) (equation (1)) and pseudo-second-order (PSO) (equation (2)) kinetic models [25] and Elovich equation (equation (3)) [26] were applied to investigate the adsorption kinetics process. Meanwhile, the intraparticle diffusion model (IPD) (equation (4)) [25] was further tested to analyze the diffusion mechanism of the adsorption.

$$\log(Q_e - Q_t) = \log(Q_e) - \frac{k_1}{2.303}t, \quad (1)$$

$$\frac{t}{Q_t} = \frac{1}{k_2 Q_e^2} + \frac{1}{Q_e}t, \quad (2)$$

$$Q_t = \beta \ln(\alpha\beta) + \beta \ln t, \quad (3)$$

$$Q_t = a + k_i t^{1/2}, \quad (4)$$

where Q_t (mg/g) and Q_e (mg/g) are the amounts of Cr(VI) adsorbed at time t (min) and at equilibrium, respectively, and k_1 (min^{-1}), k_2 (g/mg·min), k_i ($\text{mg/g·min}^{1/2}$), α (mg/g·min), and β (g/mg) are the rate constants of PFO, PSO, IPD, and Elovich equation, respectively.

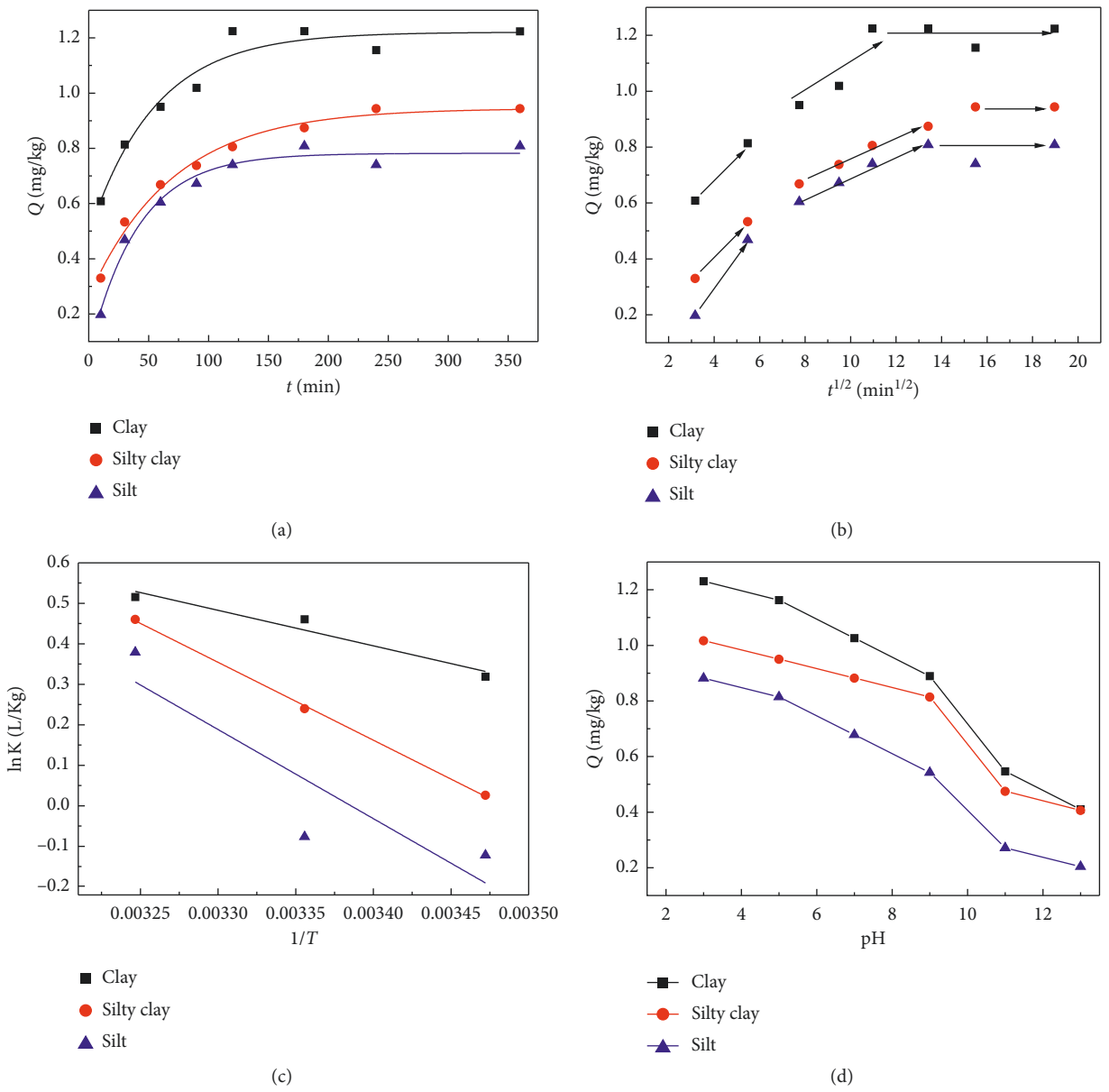

Figure 2: (a) Adsorption equilibration curves of Cr(VI) adsorption by clay, silty clay, and silt. Cr(VI) solution 1.0 mg/L, aquifers 0.1 g/mL, pH 7-8, and 288 K. (b) Intraparticle diffusion kinetics for adsorption of Cr(VI) by clay, silty clay, and silt. Cr(VI) solution 1.0 mg/L, aquifers 0.1 g/mL, pH 7-8, and 288 K. (c) Typical plots of ln K versus $1/T$ for adsorption of Cr(VI) by clay, silty clay, and silt. (d) Effect of pH on Cr(VI) adsorption by clay, silty clay, and silt. Cr(VI) solution 1.0 mg/L, aquifers 0.1 g/mL, and 288 K.

The values of different model constants are given in Table 1. The values of correlation coefficient (R^2) for the PFO kinetic model were quite low. It indicates that the adsorption of Cr(VI) onto aquifers does not follow the PFO kinetic. The values of correlation coefficient (R^2) for the PSO kinetic model were the highest. Also, the adsorption capacities calculated by the PSO kinetic model were 1.27, 1.02, and 0.87 mg/kg for clay, silty clay, and silt, respectively, which were most close to the experimental results. It indicates that the PSO model (see Supplementary Material Figure S6) was most suitable for describing the adsorption kinetics of Cr(VI) in three tested aquifers. The well-fitting PSO model suggests that the adsorption of Cr(VI) onto aquifers is highly controlled by chemisorption. Electronic forces occur between anion groups of Cr(VI) and cation groups of aquifers by sharing or exchange of electrons [27]. Similar results reported in earlier studies also showed that the PSO kinetic model was most suitable for Cr(VI) adsorption [26, 28, 29]. The experimental data also had a good fit of Elovich equation (R^2 values of 0.912–0.990). This implies a multilayer adsorption which predominates Cr(VI) adsorption in aquifers, and every layer shows various activation energy for chemisorption [30].

In addition, to better understand the adsorption mechanism, it is necessary to determine the rate-limiting step. Figure 2(b) shows that the plots are not good linear over

Table 1: Constants and coefficients of kinetic models.

Aquifers	Pseudo-first-order kinetics $\log(Q_e - Q_t) = \log(Q_e) - (k_1/2.303)t$			Pseudo-second-order kinetics $t/Q_t = (1/k_2Q_e^2) + (1/Q_e)t$			Elovich model $Q_t = \beta \ln(\alpha\beta) + \beta \ln t$			Intraparticle diffusion model $Q_t = a + k_i t^{1/2}$		
	k_1 (min^{-1})	Q_e (mg/g)	R^2	k_2 (g/mg·min)	Q_e (mg/g)	R^2	α (mg/g·min)	β (g/mg)	R^2	a	k_i (mg/g·$min^{1/2}$)	R^2
Clay	0.0215	0.83	0.455	0.1382	1.27	0.996	16.49	0.1845	0.912	0.6252	0.0380	0.775
Silty clay	0.0281	1.49	0.828	0.0376	1.02	0.998	3.575	0.1815	0.990	0.3231	0.0384	0.889
Silt	0.0276	0.82	0.617	0.0246	0.87	0.995	2.679	0.1713	0.930	0.2652	0.0334	0.753

the whole time range. It suggests more than one mechanism involved in the adsorption process [31]. Figure 2(b) shows that the IPD model fitting plots are constituted by three straight lines. The first steeper line was controlled by external surface adsorption (film diffusion); the second step with less steep was controlled by intraparticle diffusion; and the equilibrium stage was due to pore diffusion [32]. These results suggest that the adsorption mechanisms of Cr(VI) in aquifers were complex and affected by film diffusion, intraparticle diffusion, and pore diffusion. Similar findings were reported about the Cr(VI) adsorption by microporous activated carbon [33] and graphene/SiO_2@polypyrrole nanocomposites [25].

3.2.2. Adsorption Isotherm. Adsorption isotherm experiments were conducted with different initial Cr(VI) concentrations under controlled conditions of pH 7-8 and temperature 288 K, 298 K, and 308 K.

As seen in Figure 3, the adsorption capacities increased steadily with increasing initial Cr(VI) concentrations. Such a trend can be explained that the greater the quantity of Cr(VI) in the solution the higher the driving force for mass transfer to the surface of aquifers [34]. Figure 3 also shows that the adsorption of Cr(VI) in clay, silty clay, and silt all increased with increasing temperature, which implies that the adsorption process is endothermic in nature. Moreover, Figure 3 also shows that the Cr(VI) adsorption capacities of three tested aquifers varied distinctly due to their different physicochemical properties. The adsorption capacities of Cr(VI) in the three aquifers followed the order: clay > silty clay > silt.

Langmuir and Freundlich equations are the most common models in earlier studies [25, 35, 36] to describe adsorption isotherms. The Langmuir equation (equation (5)) and Freundlich equation (equation (6)) are as follows:

$$\frac{C}{Q} = \frac{1}{K_L q_m} + \frac{C}{q_m}, \tag{5}$$

$$\lg Q = \lg K_F + n \lg C, \tag{6}$$

where Q (mg/kg) is the amount of Cr(VI) adsorbed by the aquifers, C (mg/L) is the equilibrium concentration of Cr(VI), q_m (mg/kg) is the maximum adsorption capacity, K_L (L/kg) represents the Langmuir constant related to the bonding force of adsorption, K_F (L/kg) is the Freundlich adsorption equilibrium constant representing the adsorption capacity, and n is the Freundlich constant indicative of adsorption intensity.

Isotherm parameters of above described models for Cr(VI) adsorption in different aquifers at different temperatures are listed in Table 2. According to the coefficients of determination (R^2), Cr(VI) adsorption data of all tested aquifers were simultaneously better fitted by Freundlich model (Table 2). The Freundlich isotherm reflects the adsorption process occurs in a heterogeneous surface with interaction between adsorbed ions [37]. These results imply that Cr(VI) adsorption in this study was a heterogeneous multilayered adsorption [38]. Given that K_F reflects the adsorption capacity of aquifers for Cr(VI), the order of adsorption capacities was clay > silty clay > silt. As shown in Table 2, values of n were smaller than 1.0 at all temperatures, indicating that Cr(VI) is not favorably adsorbed by clay, silty clay, and silt [26]. Furthermore, the low values of K_F (Table 2) indicate that Cr(VI) is probably highly mobile in the aquifers [39]. These results suggest that Cr(VI) may transfer easily in these aquifers and cause severe pollution to the surrounding groundwater.

3.2.3. Adsorption Thermodynamics. To further clarify the adsorption mechanisms, adsorption experiments of Cr(VI) by different aquifers were carried out at 288, 298, and 308 K. The results demonstrated that the adsorption of Cr(VI) in clay, silty clay, and silt all increased with the increasing temperature (see Supplementary Material Figure S7), which is consistent with the result of the above adsorption isotherms.

The thermodynamic parameters were calculated by using the following equations:

$$\begin{aligned} \Delta G^\theta &= \Delta H^\theta - T\Delta S^\theta, \\ \Delta G^\theta &= -RT \ln K, \\ \ln K &= \frac{\Delta S^\theta}{R} - \frac{\Delta H^\theta}{RT}, \end{aligned} \tag{7}$$

where T (Kelvin) is the absolute temperature, ΔG^θ (kJ/mol) is the standard Gibbs free energy, ΔH^θ (kJ/mol) is the standard enthalpy change, ΔS^θ (J/mol·K) is the standard entropy change, and R is the gas constant (8.314 J/mol·K).

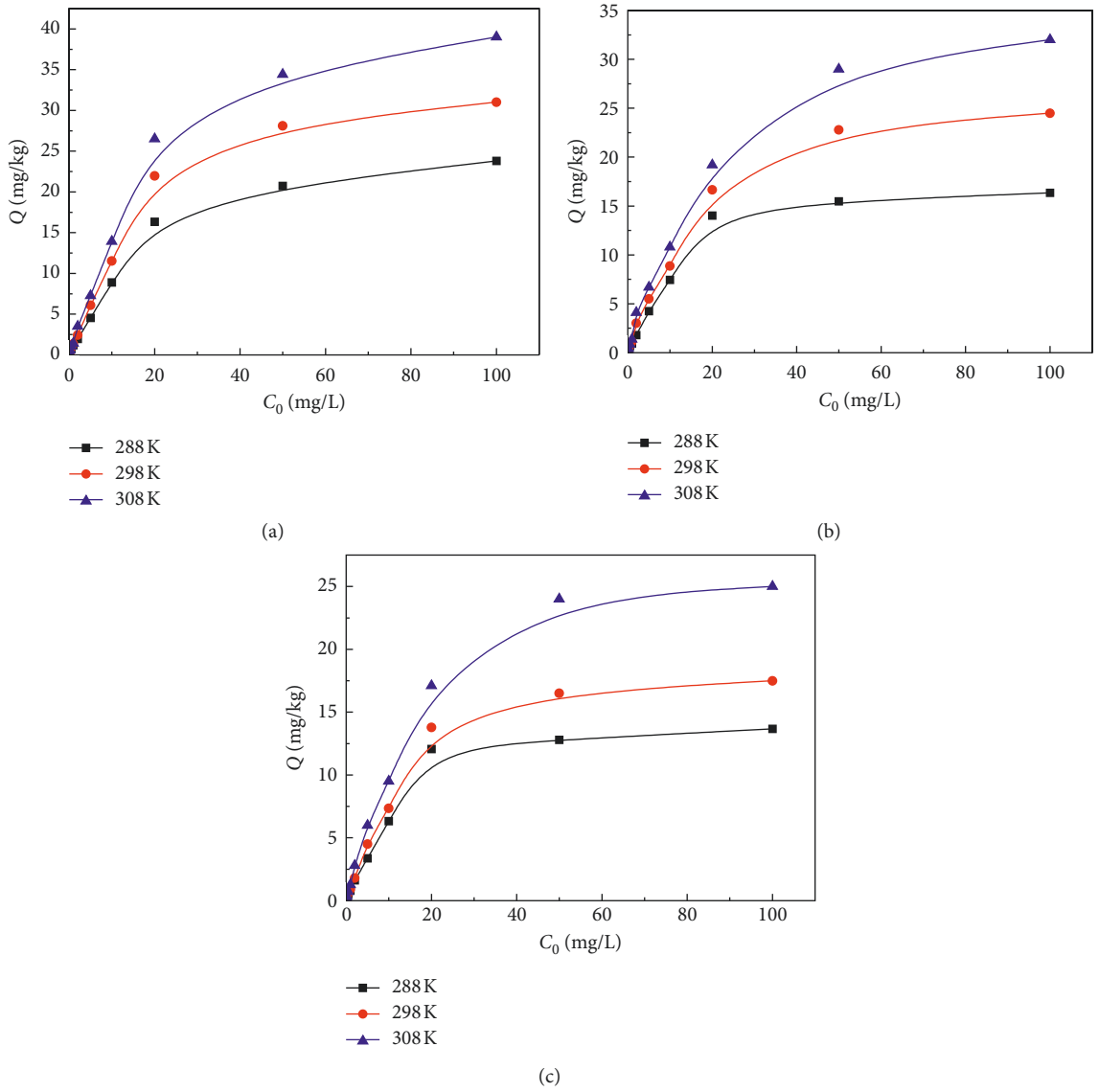

Figure 3: Adsorption isotherm curves of Cr(VI) adsorption in clay (a), silty clay (b), and silt (c).

Table 2: Isotherm parameters for adsorption of Cr(VI) in different aquifers at different temperatures.

Aquifers	Temperature (K)	Langmuir model $(C/Q) = (1/K_L q_m) + (C/q_m)$			Freundlich model $\lg Q = \lg K_F + n\lg C$		
		K_L (L/kg)	q_m (mg/kg)	R^2	K_F (L/kg)	n	R^2
Clay	288	0.057	28.33	0.907	1.438	0.751	0.991
	298	0.052	40.00	0.892	1.830	0.776	0.988
	308	0.052	49.26	0.887	2.230	0.784	0.986
Silty clay	288	0.070	20.45	0.939	1.199	0.749	0.987
	298	0.057	30.86	0.942	1.523	0.775	0.9891
	308	0.055	39.37	0.934	1.865	0.783	0.986
Silt	288	0.071	16.89	0.939	1.002	0.749	0.987
	298	0.061	22.47	0.946	1.154	0.774	0.9891
	308	0.056	32.68	0.956	1.573	0.778	0.986

ΔH^θ and ΔS^θ were computed from the slopes and intercepts of the linear regression of ln K versus $1/T$.

Thermodynamic parameters (ΔG^θ, ΔH^θ, and ΔS^θ) are present in Table 3.

Negative values of ΔG^θ (Table 3) indicate that the Cr(VI) adsorption in three tested aquifers is thermodynamically feasible and spontaneous within the temperature range 288–308 K [40]. ΔG^θ decreases with the increase in

Table 3: Thermodynamic parameters for Cr(VI) adsorption in different aquifers.

Aquifers	Temperature (K)	ΔG^{θ} (kJ/mol)	ΔH^{θ} (kJ/mol)	ΔS^{θ} (J/mol·K)
Clay	288	−0.79	7.30	28.08
	298	−1.07		
	308	−1.35		
Silty clay	288	−0.05	16.00	55.73
	298	−0.60		
	308	−1.16		
Silt	288	−0.02	18.38	62.39
	298	−0.22		
	308	−0.84		

temperature, reflecting an endothermic adsorption process. Moreover, the more negative value of ΔG^{θ} for clay indicates that more energetically favorable adsorption occurs in clay than that in silty clay and silt [41]. This phenomenon could also be explained by the higher contents of clay particles with smaller size (implies much more specific surface area), the higher average porosity (means more micropores available) [42], and the more organic matter content [43, 44] of clay than that of silty clay and silt as described in Table S4 (see Supplementary Material).

The positive enthalpy change (ΔH^{θ} ranges from 7.30 to 18.38 kJ/mol) suggests an entropy-driven process [45], which further confirms an endothermic adsorption process as observed in the aforementioned adsorption isotherms. The values of ΔH^{θ} are all less than 40 kJ/mol, suggesting a physisorption of Cr(VI) onto clay, silty clay, and silt [46]. Combined with the adsorption kinetics in earlier section, physisorption and chemisorption play important roles together in adsorption of Cr(VI) onto clay, silty clay, and silt. The values of ΔS^{θ} are positive, indicating an increased randomness at the solid-solution interface [47]. Besides, the values of ΔS^{θ} follow the sequence of clay < silty clay < silt, suggesting that the degree of randomness increases from clay to silt.

3.2.4. Effect of pH. As well known, pH plays important roles in the adsorption behavior. So, the influence of the solution pH on the Cr(VI) adsorption by three tested aquifers was investigated at 288 K and an initial Cr(VI) concentration of 1.0 mg/L. As shown in Figure 2(d), adsorption of Cr(VI) is strongly dependent on the pH; the adsorption amount of Cr(VI) in aquifers decreased with the increasing pH. The results are consistent with previous studies [17, 25, 42, 48], showing lower pH which provides more advantage for Cr(VI) adsorption. There are two main reasons for this phenomenon. Firstly, at low pH condition, large number of H^+ ions neutralize the negatively charged hydroxyl group (-OH) on the adsorbent surface, thereby reducing hindrance to the diffusion of Cr(VI) ions [25]. On the contrary, at higher pH values, the abundance of OH^- ions causes increased hindrance to diffusion of Cr(VI) ions. Secondly, the predominant form of $HCrO_4^-$ shifts to CrO_4^{2-} as pH increases [49]. $HCrO_4^-$ ion needs only one active site, whereas CrO_4^{2-} needs two active sites due to its two negative charges, thus causing a decrease of Cr(VI) adsorption as pH increases [50].

3.3. Adsorption/Desorption Columns of Cr(VI) Transport in Aquifers. In the present work, adsorption column experiments were carried out to model the contaminant transport process. In addition, the desorption column experiments were applied to model the rainwater washing the contaminant from the upper layers of soils and aquifers to subsequent depths. The breakthrough curves showed the performance of fixed-bed column. The point on the S-shaped curve at which the effluent concentration (C_t) reaches its maximum allowable value is referred as the breakthrough point [51]. The breakthrough point time and the shape of the breakthrough curve are important characteristics to determine the dynamic response of adsorption columns [52, 53].

Three breakthrough curves of adsorption columns with different aquifers are displayed in Figure 4(a). As seen from Figure 4(a), the curves all look like "S" shaped, but the slopes of the breakthrough curves change with varying aquifers. The breakthrough curves of silty clay and silt are steeper than that of clay, which may be explained on the mass transfer fundamentals [53]. A slower transport of Cr(VI) in clay could be caused by a decrease in mass transfer coefficient or diffusion coefficient [54, 55]. Moreover, this result also supported the aforementioned adsorption kinetics study. As illustrated in Table S4 (see Supplementary Material), more clay particles (means more adsorbent surface area) and more organic matter content in clay column provided more binding sites with Cr(VI), indicating a relatively slow transfer process. Also, the organic matter in the aquifers may have reduced some Cr(VI) into Cr(III), greatly reducing the transport of Cr(VI) through the aquifers [16, 56, 57]. Considering that the porosity of the packed column (Table S3) is higher than the actual porosity of study site (Table S4), it could be inferred that the seepage velocity of Cr(VI) in the actual aquifers is slower.

On the other hand, the breakthrough curves of desorption columns are shown in Figure 4(b). The results showed that the concentrations of Cr(VI) in three kinds of columns of aquifers all decreased with time (Figure 4(b)). It demonstrated that the Cr(VI) adsorbed on aquifers will desorb and release into groundwater day by day in the case of rainwater leaching, causing groundwater recontamination. Meanwhile, the curve slopes of silty clay and silt columns were steeper than that of clay column, and the breakthrough curve of clay showed a strong trailing phenomenon. It suggests that the desorption process of clay

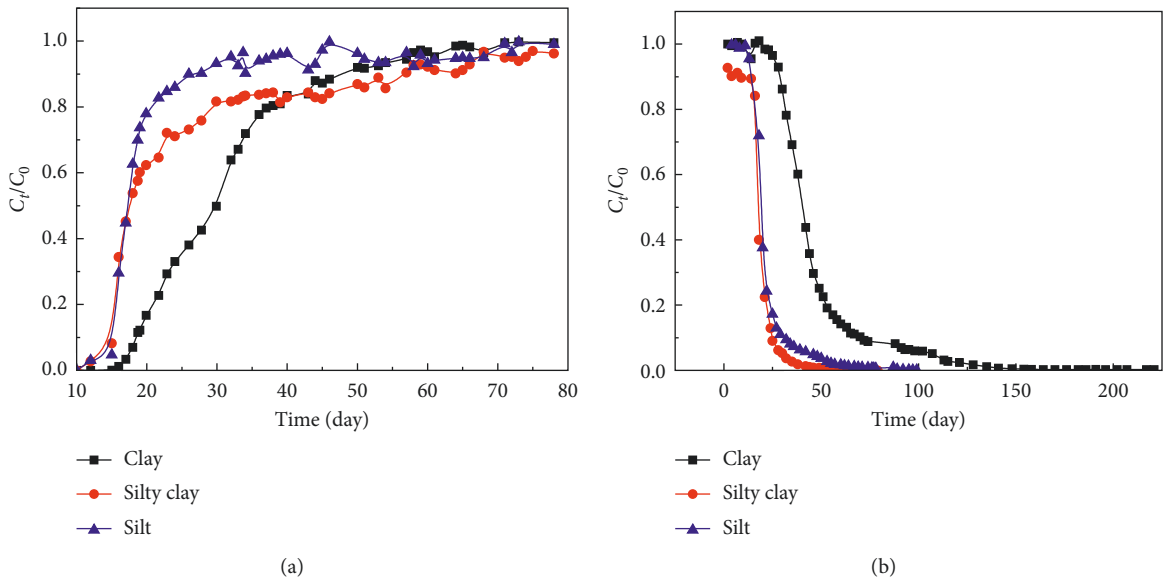

Figure 4: Breakthrough curves of adsorption columns (a) and desorption columns (b).

column is much slower than that of silty clay and silt columns. This result is also consistent with aforementioned results of adsorption isotherms.

Finally, according to the result of adsorption and desorption column experiments, the COPR leachate will continuously transport into aquifers and groundwater therefore causing severe pollution. At the same time, the chromium adsorbed on the aquifers will desorb and release into groundwater under the action of rainwater leaching, causing a recontamination of groundwater. Therefore, the COPR dumpsite is urgent to be properly treated. Also, comprehensive management of soils must be attached importance to prevent any further pollution of groundwater.

4. Conclusions

The results from this study are summarized as follows:

(1) The top soils (5–10 cm), shallow aquifers, and groundwater nearby the chromium ore processing residue (COPR) dumpsite are severely polluted by Cr(VI).

(2) The adsorption of Cr(VI) in aquifers was well described by pseudo-second-order kinetics equations and Freundlich model. The kinetic results proved that Cr(VI) is not easily adsorbed by aquifer mediums but transports with groundwater, causing long-distance pollution. The adsorption capacities of Cr(VI) in three tested aquifers followed the order: clay > silty clay > silt. Cr(VI) adsorption capacities in three tested aquifers decreased with increasing pH.

(3) Different thermodynamic parameters such as ΔG^{θ}, ΔH^{θ}, and ΔS^{θ} showed that the adsorption of Cr(VI) onto tested aquifers was feasible, spontaneous, and endothermic in nature. Adsorption kinetic and thermodynamic results imply that physisorption and chemisorption play important roles together in the Cr(VI) adsorption onto clay, silty clay, and silt.

(4) Breakthrough curves of adsorption columns with different aquifers showed that the transport of Cr(VI) followed the sequence of clay < silty clay < silt.

(5) Desorption column experiments infer that the Cr(VI) adsorbed on aquifers will desorb and release into groundwater in the case of rainwater leaching, causing groundwater recontamination.

Data Availability

The data used to support the findings of this study are available from the corresponding author upon request.

Conflicts of Interest

The authors declare no conflicts of interest.

Acknowledgments

This work was supported by the Science and Technology Project of Tianjin Water Bureau (no. KY2014-03). The authors also gratefully acknowledge the support from the National Science Foundation of China (no. 41807386).

Supplementary Materials

The detailed information of sampling, soil characteristics, and experiments are described in the Supplementary Material. Photos of chromium ore processing residue (COPR) dumpsite in the former Tianjin Tongsheng Chemical Factory in 2012 (Figure S1). Photos of core drilling and groundwater sampling (Figure S2). Schematic of adsorption column packed with aquifers (Figure S3). The concentrations of total

Cr in top soils (5–10 cm) of 11 sampling sites (Figure S4). The concentrations of total Cr in aquifers at different depths of 1–6 m of 11 sampling sites (Figure S5). Pseudo-second-order kinetics for adsorption of Cr(VI) onto clay, silty clay, and silt. Cr(VI) solution 1.0 mg/L, aquifers 0.1 g/mL, pH 7-8, and 288 K (Figure S6). Effect of temperature on Cr(VI) adsorption by clay, silty clay, and silt. Cr(VI) solution 1.0 mg/L, aquifers 0.1 g/mL, and pH 7-8 (Figure S7). Geographical locations of the drilling sampling sites (Table S1).Vertical distribution of local geological formations (Table S2). Packing status of columns and operating condition for the adsorption/desorption column study (Table S3). The physicochemical properties of different aquifers (Table S4). The concentration of Cr(VI) and total Cr of groundwater in monitoring wells of 11 sampling sites (Table S5). (*Supplementary Materials*)

References

[1] B. A. Marinho, R. O. Cristóvão, R. Djellabi et al., "Strategies to reduce mass and photons transfer limitations in heterogeneous photocatalytic processes: hexavalent chromium reduction studies," *Journal of Environmental Management*, vol. 217, pp. 555–564, 2018.

[2] L. Zhong and J. Yang, "Reduction of Cr(VI) by malic acid in aqueous Fe-rich soil suspensions," *Chemosphere*, vol. 86, no. 10, pp. 973–978, 2012.

[3] L. J. D. Moreira, E. B. Da Silva, M. P. F. Fontes, X. Liu, and L. Q. Ma, "Speciation, bioaccessibility and potential risk of chromium in Amazon forest soils," *Environmental Pollution*, vol. 239, pp. 384–391, 2018.

[4] H. Lyu, H. Zhao, J. Tang et al., "Immobilization of hexavalent chromium in contaminated soils using biochar supported nanoscale iron sulfide composite," *Chemosphere*, vol. 194, pp. 360–369, 2018.

[5] J. Johnson, L. Schewel, and T. E. Graedel, "The contemporary anthropogenic chromium cycle," *Environmental Science & Technology*, vol. 40, no. 22, pp. 7060–7069, 2006.

[6] C. V. Coller-Myburgh, L. V. Rensburg, and M. Maboeta, "Utilizing earthworm and microbial assays to assess the ecotoxicity of chromium mine wastes," *Applied Soil Ecology*, vol. 83, pp. 258–265, 2014.

[7] USEPA, *Edition of the Drinking Water Standards and Health Advisories*, Office of Water, U.S. Environmental Protection Agency, Washington, DC, USA, 2012.

[8] R. A. Fallahzadeh, R. Khosravi, B. Dehdashti et al., "Spatial distribution variation and probabilistic risk assessment of exposure to chromium in ground water supplies; a case study in the east of Iran," *Food and Chemical Toxicology*, vol. 115, pp. 260–266, 2018.

[9] J. S. Geelhoed, J. C. L. Meeussen, M. J. Roe et al., "Chromium remediation or release? Effect of iron(II) sulfate addition on chromium(VI) leaching from columns of chromite ore processing residue," *Environmental Science & Technology*, vol. 37, no. 14, pp. 3206–3213, 2003.

[10] H. S. Shi and L. L. Kan, "Study on the properties of chromium residue-cement matrices (CRCM) and the influences of superplasticizers on chromium(VI)-immobilising capability of cement matrices," *Journal of Hazardous Materials*, vol. 162, no. 2-3, pp. 913–919, 2009.

[11] X. Zhao, P. A. Sobecky, L. Zhao, P. Crawford, and M. Li, "Chromium(VI) transport and fate in unsaturated zone and aquifer: 3D Sandbox results," *Journal of Hazardous Materials*, vol. 306, pp. 203–209, 2016.

[12] T. Sherene, "Mobility and transport of heavy metals in polluted soil environment," *Biological Forum-An International Journal*, vol. 2, no. 2, pp. 112–121, 2010.

[13] C.-H. Weng, C. P. Huang, and P. F. Sanders, "Transport of Cr(VI) in soils contaminated with chromite ore processing residue (COPR)," *Practice Periodical of Hazardous, Toxic, and Radioactive Waste Management*, vol. 6, no. 1, pp. 6–13, 2002.

[14] A. A. Khan, M. Muthukrishnan, and B. K. Guha, "Sorption and transport modeling of hexavalent chromium on soil media," *Journal of Hazardous Materials*, vol. 174, no. 1–3, pp. 444–454, 2010.

[15] J. Jiang, R. Xu, Y. Wang, and A. Zhao, "The mechanism of chromate sorption by three variable charge soils," *Chemosphere*, vol. 71, no. 8, pp. 1469–1475, 2008.

[16] P. M. Jardine, S. E. Fendorf, M. A. Mayes, I. L. Larsen, S. C. Brooks, and W. B. Bailey, "Fate and transport of hexavalent chromium in undisturbed heterogeneous soil," *Environmental Science & Technology*, vol. 33, no. 17, pp. 2939–2944, 1999.

[17] D. M. Dong, X. M. Zhao, X. Y. Hua, J. Liu, and G. Ming, "Investigation of the potential mobility of Pb, Cd and Cr(VI) from moderately contaminated farmland soil to groundwater in Northeast, China," *Journal of Hazardous Materials*, vol. 162, no. 2-3, pp. 1261–1268, 2009.

[18] D. B. Kent, J. A. Davis, L. C. D. Anderson, and B. A. Rea, "Transport of chromium and selenium in a pristine sand and gravel aquifer: role of adsorption processes," *Water Resources Research*, vol. 31, no. 4, pp. 1041–1050, 1995.

[19] D. B. Kent, J. A. Davis, L. C. D. Anderson, B. A. Rea, and T. D. Waite, "Transport of chromium and seleniumin the suboxicz one of a shallow aquifer: influence of redox and adsorption reactions," *Water Resources Research*, vol. 30, no. 4, pp. 1099–1114, 1994.

[20] China MC, *Standard for Engineering Classification of Soil*, Ministry of Construction of China, Beijing, China, 2007, in Chinese.

[21] TCMC, *Technical Specification for Division of Subsoil Sequence in Tianjin*, Tianjin Construction Management Committee, Tianjin, China, 2009, in Chinese.

[22] China MEE, "Environmental quality standard for soils," Ministry of Ecology and Environmental of China, Beijing, China, 2018, in Chinese.

[23] X. Liu, J. Jiang, Y. Yan et al., "Distribution and risk assessment of metals in water, sediments, and wild fish from Jinjiang River in Chengdu, China," *Chemosphere*, vol. 196, pp. 45–52, 2018.

[24] China MEE, "Quality standard for groundwater," Ministry of Ecology and Environmental of China, Beijing, China, 2017, in Chinese.

[25] W. Fang, X. Jiang, H. Luo, and J. Geng, "Synthesis of graphene/SiO_2@polypyrrole nanocomposites and their application for Cr(VI) removal in aqueous solution," *Chemosphere*, vol. 197, pp. 594–602, 2018.

[26] K. L. Tan and B. H. Hameed, "Insight into the adsorption kinetics models for the removal of contaminants from aqueous solutions," *Journal of the Taiwan Institute of Chemical Engineers*, vol. 74, pp. 25–48, 2017.

[27] J.-H. Park, J. J. Wang, R. Xiao et al., "Mercury adsorption in the Mississippi River deltaic plain freshwater marsh soil of Louisiana Gulf coastal wetlands," *Chemosphere*, vol. 195, pp. 455–462, 2018.

[28] N. Li, F. Fu, J. Lu, Z. Ding, B. Tang, and J. Pang, "Facile preparation of magnetic mesoporous $MnFe_2O_4$@SiO_2-CTAB composites for Cr(VI) adsorption and reduction," *Environmental Pollution*, vol. 220, pp. 1376–1385, 2017.

[29] S. Mallick, S. S. Dash, and K. M. Parida, "Adsorption of hexavalent chromium on manganese nodule leached residue obtained from NH_3-SO_2 leaching," *Journal of Colloid and Interface Science*, vol. 297, no. 2, pp. 419–425, 2006.

[30] M. Omidvar Borna, M. Pirsaheb, M. Vosoughi Niri et al., "Batch and column studies for the adsorption of chromium(VI) on low-cost Hibiscus Cannabinus kenaf, a green adsorbent," *Journal of the Taiwan Institute of Chemical Engineers*, vol. 68, pp. 80–89, 2016.

[31] A. Kumar and H. M. Jena, "Adsorption of Cr(VI) from aqueous phase by high surface area activated carbon prepared by chemical activation with $ZnCl_2$," *Process Safety and Environmental Protection*, vol. 109, pp. 63–71, 2017.

[32] W. Zhang, S. Zhang, J. Wang et al., "Hybrid functionalized chitosan-Al_2O_3@SiO_2 composite for enhanced Cr(VI) adsorption," *Chemosphere*, vol. 203, pp. 188–198, 2018.

[33] R. Gottipati and S. Mishra, "Preparation of microporous activated carbon from *Aegle Marmelos* fruit shell and its application in removal of chromium(VI) from aqueous phase," *Journal of Industrial and Engineering Chemistry*, vol. 36, pp. 355–363, 2016.

[34] A. Iriel, S. P. Bruneel, N. Schenone, and A. F. Cirelli, "The removal of fluoride from aqueous solution by a lateritic soil adsorption: kinetic and equilibrium studies," *Ecotoxicology and Environmental Safety*, vol. 149, pp. 166–172, 2018.

[35] J. O. Vinhal, K. K. Nege, M. R. Lage, J. W. M. Carneiro, C. F. Lima, and R. J. Cassella, "Adsorption of of the herbicides diquat and difenzoquat on polyurethane foam: kinetic, equilibrium and computational studies," *Ecotoxicology and Environmental Safety*, vol. 145, pp. 597–604, 2017.

[36] L. A. Holmes, A. Turner, and R. C. Thompson, "Adsorption of trace metals to plastic resin pellets in the marine environment," *Environmental Pollution*, vol. 160, pp. 42–48, 2012.

[37] A. El Nemr, A. Khaled, O. Abdelwahab, and A. El-Sikaily, "Treatment of wastewater containing toxic chromium using new activated carbon developed from date palm seed," *Journal of Hazardous Materials*, vol. 152, no. 1, pp. 263–275, 2008.

[38] B. Fuentes, M. de la Luz Mora, R. Bol, F. San Martin, E. Pérez, and P. Cartes, "Sorption of inositol hexaphosphate on desert soils," *Geoderma*, vol. 232–234, pp. 573–580, 2014.

[39] K. M. Doretto and S. Rath, "Sorption of sulfadiazine on Brazilian soils," *Chemosphere*, vol. 90, no. 6, pp. 2027–2034, 2013.

[40] M. Jain, V. K. Garg, and K. Kadirvelu, "Adsorption of hexavalent chromium from aqueous medium onto carbonaceous adsorbents prepared from waste biomass," *Journal of Environmental Management*, vol. 91, no. 4, pp. 949–957, 2010.

[41] X. Guo, C. Yang, Z. Dang, Q. Zhang, Y. Li, and Q. Meng, "Sorption thermodynamics and kinetics properties of tylosin and sulfamethazine on goethite," *Chemical Engineering Journal*, vol. 223, pp. 59–67, 2013.

[42] Z. A. Zakaria, M. Suratman, N. Mohammed, and W. Azlina Ahmad, "Chromium(VI) removal from aqueous solution by untreated rubber wood sawdust," *Desalination*, vol. 244, no. 1–3, pp. 109–121, 2009.

[43] X. Zhang, J. Tong, B. X. Hu, and W. Wei, "Adsorption and desorption for dynamics transport of hexavalent chromium (Cr(VI)) in soil column," *Environmental Science and Pollution Research*, vol. 25, no. 1, pp. 459–468, 2018.

[44] D. A. Brose and B. R. James, "Hexavalent chromium reduction by tartaric acid and isopropyl alcohol in mid-atlantic soils and the role of Mn(III, IV)(hydr)oxides," *Environmental Science & Technology*, vol. 47, no. 22, pp. 12985–12991, 2013.

[45] J. Yang, M. Yu, and W. Chen, "Adsorption of hexavalent chromium from aqueous solution by activated carbon prepared from longan seed: kinetics, equilibrium and thermodynamics," *Journal of Industrial and Engineering Chemistry*, vol. 21, pp. 414–422, 2015.

[46] M. Kara, H. Yuzer, E. Sabah, and M. S. Celik, "Adsorption of cobalt from aqueous solutions onto sepiolite," *Water Research*, vol. 37, no. 1, pp. 224–232, 2003.

[47] J. Maszkowska, M. Wagil, K. Mioduszewska, J. Kumirska, P. Stepnowski, and A. Białk-Bielińska, "Thermodynamic studies for adsorption of ionizable pharmaceuticals onto soil," *Chemosphere*, vol. 111, pp. 568–574, 2014.

[48] S. R. Chowdhury and E. K. Yanful, "Arsenic and chromium removal by mixed magnetite-maghemite nanoparticles and the effect of phosphate on removal," *Journal of Environmental Management*, vol. 91, no. 11, pp. 2238–2247, 2010.

[49] T. Shanthi and V. M. Selvarajan, "Removal of Cr(VI) and Cu(II) ions from aqueous solution by carbon prepared from henna leaves," *Journal of Chemistry*, vol. 2013, Article ID 304970, 6 pages, 2013.

[50] J. Yang, M. Yu, and T. Qiu, "Adsorption thermodynamics and kinetics of Cr(VI) on KIP210 resin," *Journal of Industrial and Engineering Chemistry*, vol. 20, no. 2, pp. 480–486, 2014.

[51] S. Kundu, S. S. Kavalakatt, A. Pal, S. K. Ghosh, M. Mandal, and T. Pal, "Removal of arsenic using hardened paste of Portland cement: batch adsorption and column study," *Water Research*, vol. 38, no. 17, pp. 3780–3790, 2004.

[52] R. P. Han, Y. Wang, X. Zhao et al., "Adsorption of methylene blue by phoenix tree leaf powder in a fixed-bed column: experiments and prediction of breakthrough curves," *Desalination*, vol. 245, no. 1–3, pp. 284–297, 2009.

[53] A. A. Ahmad and B. H. Hameed, "Fixed-bed adsorption of reactive azo dye onto granular activated carbon prepared from waste," *Journal of Hazardous Materials*, vol. 175, no. 1–3, pp. 298–303, 2010.

[54] M. T. Uddin, M. Rukanuzzaman, M. M. R. Khan, and I. Akhtarul, "Adsorption of methylene blue from aqueous solution by jackfruit (*Artocarpus heteropyllus*) leaf powder: a fixed-bed column study," *Journal of Environmental Management*, vol. 90, no. 11, pp. 3443–3450, 2009.

[55] N. Chen, Z. Y. Zhang, C. P. Feng, L. Miao, C. Rongzhi, and N. Sugiura, "Investigations on the batch and fixed-bed column performance of fluoride adsorption by Kanuma mud," *Desalination*, vol. 268, no. 1–3, pp. 76–82, 2011.

[56] J. L. Gardea-Torresday, K. J. Tiemann, V. Armendariz et al., "Characterization of Cr(VI) binding and reduction to Cr(III) by the agricultural byproducts of *Avena monida* (Oat) biomass," *Journal of Hazardous Materials*, vol. 80, no. 1–3, pp. 175–188, 2000.

[57] N.-H. Hsu, S.-L. Wang, Y.-C. Lin, G. D. Sheng, and J.-F. Lee, "Reduction of Cr(VI) by crop-residue-derived black carbon," *Environmental Science & Technology*, vol. 43, no. 23, pp. 8801–8806, 2009.